Research Article

Assessing the impact of Argo float temperature measurements on the forecast skill of a weather prediction numerical model

George VARLAS[1,2], Petros KATSAFADOS[1], Gerasimos KORRES[3] and Anastasios PAPADOPOULOS[2]

[1] Department of Geography, Harokopio University of Athens (HUA), El. Venizelou Str. 70, 17671 Athens, Greece

[2] Institute of Marine Biological Resources and Inland Waters, Hellenic Centre for Marine Research (HCMR), 46.7 Km Athens-Sounio avenue, 19013 Anavissos, Attica, Greece

[3] Institute of Oceanography, HCMR, 46.7 Km Athens-Sounio avenue, 19013 Anavissos, Attica, Greece

Corresponding author: pkatsaf@hua.gr

Handling Editor: Takvor SOUKISSIAN

Abstract

The forecast skill of numerical weather prediction (NWP) models relies, among other factors such as the prediction itself and the assimilation scheme, on the accuracy of the observations utilized in the assimilation systems for the production of initial and boundary conditions. One of the most crucial parameters in weather forecasting is the sea surface temperature (SST). In the majority of NWP models, the initial and lower boundary conditions involve gridded (SST) analyses, which consist of data obtained by buoys, ships and satellites. The main aim of this study is to integrate Argo temperature measurements in gridded SST analyses and to assess their impact on the forecast skill of a limited area atmospheric model. Argo floats are "state-of-the-art" oceanographic instruments producing high-quality temperature profiles for the ice-free ocean. In this study, Argo temperatures are incorporated into gridded SST fields without applying any smoothing method in order to assess directly the impact of Argo temperatures on numerical weather prediction. Their impact is assessed under intense weather cyclonic conditions in the Mediterranean Sea by performing two sensitivity simulations, either incorporating or not Argo temperatures in gridded SST fields used for the generation of the initial and lower boundary conditions. The results indicate that the inclusion of Argo-measured near-surface temperatures in the lower boundary condition modifies the surface heat fluxes, thus affecting mean sea level pressure and precipitation. In particular, an overall improvement of the precipitation forecast skill of up to 3% has been demonstrated. Moreover, the incorporation of Argo temperatures affects the simulated track and intensity of the cyclone over the Balkan Peninsula.

Keywords: Argo floats; RTG; SST; numerical weather prediction; atmospheric modelling; WRF-ARW.

Introduction

The performance of numerical weather prediction (NWP) models depends on both the efficient solution of physical equations and the quality of the observation data used for the generation of initial and boundary conditions (Mohanty *et al*., 2010; Gopalakrishnan *et al*., 2012; Pielke, 2013). Sea surface temperature (SST) is one of the most important fields of the lower boundary conditions in atmospheric simulations (Katsafados *et al*., 2005; 2011). The majority of NWP models utilize gridded SST analyses, consisting of properly blended buoy, ship and satellite-derived data (Reynolds *et al*., 2002; Thiébaux *et al*., 2003; Gemmill *et al*., 2007; Kara & Barron, 2007).

In recent years, *in-situ* ocean temperature measurements present an increasing trend in efforts to cover wide areas of the world oceans. In particular, profiling floats are characterized by the capability to produce accurate temperature profiles for oceans with the exception of iced areas (The Argo Science Team, 1998; Roemmich & Gilson, 2009). The international ARGO program for the Oceans was initiated in 1999 as a pilot project endorsed by the Climate Research Program of the World Meteorological Organization and the Intergovernmental Oceanographic Commission. At global scale, deployments began in year 2000 and continue today at a rate of about 800 per year. More information is available in Argo (2000) and at http://www.argo.ucsd.edu. The Argo float array is an important tool used for the initialization, data assimilation and performance assessment of oceanic models (Tonani *et al*., 2014). Moreover, Argo near surface temperature measurements can play a crucial role in the improvement of SST analyses and, consequently, of numerical weather prediction.

The Euro-Argo project started in January 2008 and aims at developing European infrastructure for Argo provided that European partners have the capacity to procure

Medit. Mar. Sci., 20/2, 2019, 331-341

331

and deploy about 250 floats per year, monitor such floats and ensure that all the data can be processed and delivered to users (both in real-time and delayed-mode). With a mean float lifetime of 2 years, such a European contribution would support approximately 25% of the global array and additionally provide 50 floats per year for enhanced coverage of the European Seas (e.g. the Nordic, Mediterranean and Black Seas). The Euro-Argo project involves 25 organizations from 12 European countries and aims to enhance the collective ability of European nations to contribute to Argo, while improving the understanding of the physical mechanisms in European Seas. More information is available in Le Traon (2013) and at http://www.euro-argo.eu.

Within the framework of the Mediterranean Argo (MedArgo) project, Greece supports Argo infrastructure and research activities with an increasing number of deployed floats [more information is available in Kassis *et al*. (2014) and at http://www.greekargo.gr], thus improving the description and analysis of the circulation characteristics and thermohaline structure in the Aegean and Ionian Seas (Krokos *et al*., 2014; Velaoras *et al*., 2014; Kassis *et al*., 2015, 2016, 2017). In 2010, the Hellenic Centre for Marine Research (HCMR) procured and deployed a float to initiate the Greek Argo program. The first float was deployed in the Cretan Sea, south of Santorini Island on 26 June 2010 (Korres & Kassis, 2012). In June 2017, there were 6 Greek floats in the Aegean and southern Ionian Seas (Fig. 1). The raw measurements of the Greek floats are delivered to the Coriolis data Centre where they are subjected to real-time quality control while the delayed mode quality control of the data is performed by the MedArgo Centre of the Istituto Nazionale di Oceanografia e di Geofisica Sperimentale (OGS). The Argo metadata is freely available through the Coriolis data Centre (http://www.coriolis.eu.org) and the database of the European Commission Copernicus project (http://marine.copernicus.eu).

In general, Argo data are mainly used for model evaluation and data assimilation systems in ocean circulation models, as well as the study of ocean heat content and its variability. Many studies related to Argo data assimilation in ocean circulation models (e.g. Xie *et al*., 2010; Nilsson *et al*., 2011; Mignac *et al*., 2015) have revealed improvement as regards their forecast skill. In particular, MedArgo data are routinely assimilated (using localized Singular Evolutive Extended Kalman filtering techniques) on a weekly basis in one of the operational forecasting systems that are currently operating at HCMR, involving the Mediterranean basin, 1/10° resolution (POSEIDON system), and the Aegean Sea, 1/30° resolution (Korres *et al*., 2009; Korres *et al*., 2010; Korres & Kassis, 2012). MedArgo data have also been used as independent data for assessing the impact of remotely sensed and Ferrybox SST and Sea Surface Salinity (SSS) data assimilation into the hydrodynamic component of the POSEIDON system operationally running at HCMR (Korres *et al*., 2014).

Apart from the exploitation of Argo data in ocean circulation models, the assimilation of Argo temperatures in SST analyses and their impact on numerical weather prediction is already assessed through a global-seasonal approach. Argo temperatures have improved the ECMWF (European Centre for Medium Range Weather Forecasts) SST analyses and the seasonal forecast skill of the ECMWF atmosphere-ocean coupled system, although error reduction was limited (Balmaseda *et al*., 2007; Balmaseda & Anderson, 2009).

Thus, the main aim of this study is to expand the integration of MedArgo temperature measurements to limited area atmospheric simulations and to investigate the sensitivity of atmospheric response. This is accomplished by integrating upper-sea MedArgo temperatures onto gridded SST analysis fieldss used for the generation of initial and lower boundary conditions of atmospheric simulations. The impact of the MedArgo temperatures on the forecast skill of an advanced limited area atmospheric model is assessed by performing a pair of simulations for an extreme weather event over the Mediterranean Sea.
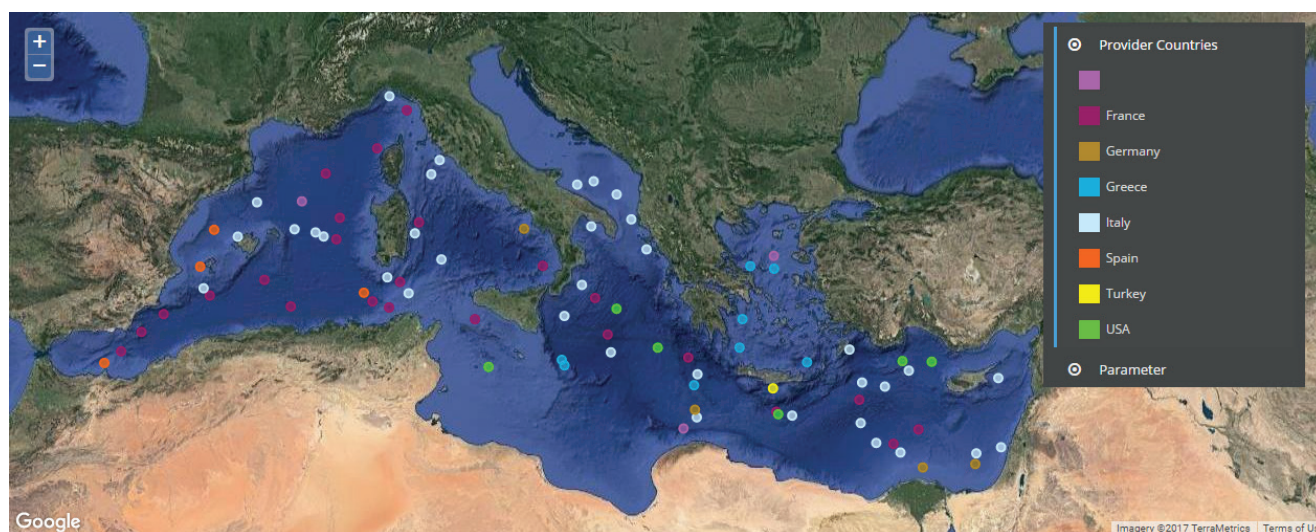

Fig. 1: Distribution of active Mediterranean floats in the Argo array, colour-coded per country owning the float, in June 2017 (http://www.greekargo.gr/).

332

Medit. Mar. Sci., 20/2, 2019, 331-341

Description of the extreme weather event

The selected case study is characterized by the formation of two cyclonic systems over the central and eastern Mediterranean Sea during the period from 29 January to 3 February 2015 (Varlas *et al.*, 2018c). In more detail, on 29 January 2015 at 12:00 UTC a cut-off upper-level trough supported the generation of a barometric low over the southern Ionian Sea that mostly affects south-western Greece (Fig. 2a, 3a). Meanwhile, a new barometric low was generated over the Ligurian Sea (Fig. 2b). This system deepened by the southward invasion of an upper-level trough from central Europe (Fig. 3b). On 30 January at 12:00 UTC, minimum mean sea level pressure (MSLP) of the low dropped to 974 hPa over north-eastern Italy. In the next days, the barometric system expanded from Italy to Greece and was accompanied by fronts, which supported persistent torrential rainfall (Fig. 2c, 3c). The trough covered a widespread part of the Mediterranean Sea and remained almost stagnant for many hours (Fig. 3d). This supported the slow passage of fronts over Italy and Greece until 2 February, triggering consecutive gale force winds and heavy rainfall (Fig. 2b, c, d). It is noteworthy that the phenomena were characterized by increased intensity and duration mainly over western and central Greece, causing flash floods and damages.

Model configuration and simulation setup

The impact of Argo temperatures on atmospheric conditions is assessed by employing the Advanced Weather Research (ARW) core of the Weather Research and Forecasting (WRF) version 3.6 model (Skamarock *et al.*, 2008) to simulate the particular extreme weather event,

either taking into account the Argo measurements near the sea surface or not. The WRF-ARW model was selected due to its advanced capabilities to resolve atmospheric processes (Christakos *et al.*, 2014, 2016; Varlas *et al.*, 2018b; Katsafados *et al.*, 2018). WRF-ARW is a fully compressible and non-hydrostatic numerical mesoscale model. It uses the Arakawa semi-staggered C-grid and a terrain-following hydrostatic pressure coordinate. The numerical experiments are performed on a 516 × 294 horizontal grid covering the Mediterranean Sea, a widespread part of Europe and the north part of Africa with a horizontal resolution of 10 km × 10 km (Fig. 4). Moreover, a time step of 60 s and 38 vertical levels stretching from the surface to 50 hPa are used. The initial and boundary conditions are based on the Global Forecasting System (GFS) operational analyses with a horizontal resolution of 0.5° × 0.5° involving 20 isobaric levels and 4 soil layers. The initial SST field is based on the high-resolution (0.083° × 0.083°) Real Time Global (RTG) SST analyses operationally produced by the National Centers for Environmental Prediction/Marine Modeling and Analysis Branch (NCEP/MMAB) sin ce 2005. RTG SST analyses are generated every day at 00:00 UTC using two-dimensional variational interpolation analysis of the most recent 24-hours in-situ (fixed and drifting buoys as well as some ships) and satellite-retrieved (NOAA-17 and NOAA-18) data considering sea ice cover (Thiébaux *et al.*, 2003; Gemmill *et al.*, 2007). Moreover, it is important to note that the RTG SST analyses actually correspond to temperatures representative of the upper layer of the ocean and not exactly to SSTs (more information is available at http://polar.ncep.noaa.gov/sst).

For short simulations, like the present case study, the SST field is defined at the initial time and usually remains constant throughout the simulation. In this study,
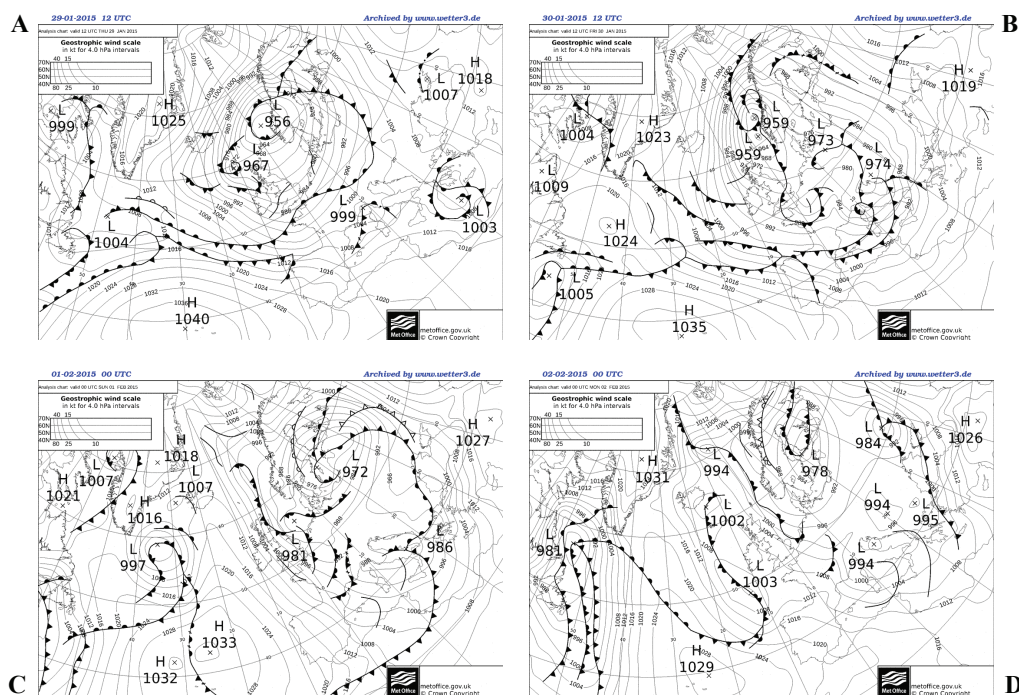

Fig. 2: Surface pressure analysis map (mb) for a) 29 January at 12:00 UTC b) 30 January at 12:00 UTC b) 1 February at 00:00 UTC b) 2 February at 00:00 UTC, 2015. Maps provided courtesy of the UK Met Office surface analysis archive.
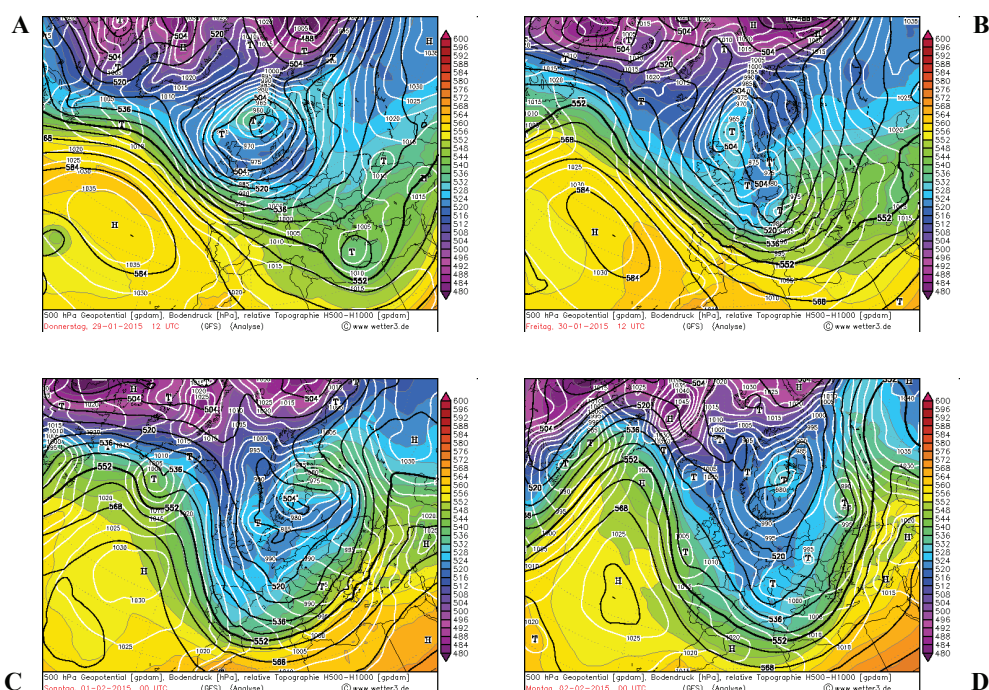
Medit. Mar. Sci., 20/2, 2019, 331-341

333

Fig. 3: Mean Sea Level Pressure (white contours in hPa), geopotential height at 500 hPa (black contours in gpm) and thickness 1000-500 hPa (colour-shaded in gpm) for (a) 29 January at 12:00 UTC (b) 30 January at 12:00 UTC (b) 1 February at 00:00 UTC b) 2 February at 00:00 UTC, 2015. Maps provided courtesy of www.wetter.de archive.
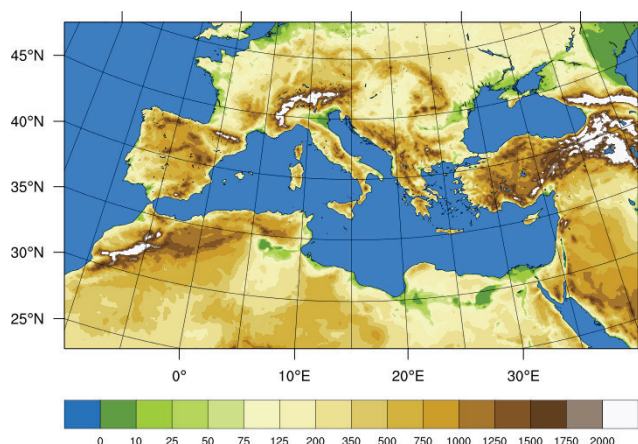

Fig. 4: Simulations domain and topography (m).

however, the SST has been updated periodically in order to investigate model sensitivity to time-varying SST. In particular, SST was updated every 6 hours during the simulation, directly based on the RTG analyses for 00:00 UTC and performing temporal interpolation for the middle times (06:00, 12:00 and 18:00 UTC). The main configuration characteristics of WRF-ARW and the parameterization schemes employed in the simulation of the extreme weather conditions are listed in Table 1.

Two sensitivity simulations are designed to investigate the impact of Argo temperatures on the simulation of the extreme weather event. The first (hereafter referred to as CTRL) employs only RTG analyses for the generation of the initial and lower boundary conditions over the sea and the second (hereafter: ARGO) additionally integrates the available Argo temperatures. The methodology applied for Argo temperature incorporation in the

Table 1. Main configuration characteristics of WRF-ARW and parameterization schemes employed in the sensitivity simulations.

WRF-ARW	Configuration characteristics & parameterization schemes
Grid	Arakawa semi-staggered C-grid
Horizontal grid increment	10 km x 10 km
Vertical coordinate	Terrain-following hydrostatic pressure coordinate
Vertical levels	38
Time step	60 s
Initial & boundary conditions	GFS, 0.5° x 0.5°, 20 isobaric levels, 4 soil layers, 6-hour update of boundary conditions
SST	GFS, 6-hour SST update
Microphysics	WRF Single-Moment 3-class (Hong *et al*., 2004)
Planetary Boundary Layer	Yonsei University (YSU) [Hong *et al*., 2006]
Surface Layer	Revised Monin-Obukhov (Jiménez *et al*., 2012)
Land Surface	Unified Noah land-surface model (Tewari *et al*., 2004)

RTG analyses is based on spatial and temporal interpolation schemes. Argo temperatures are distributed using a 6-hour time frame (±3 hours from the time) in order to match the SST update times (00:00, 06:00, 12:00 and 18:00 UTC). For example, the corresponding Argo temperatures on 29 January at 00:00 UTC cover the time period from 28 January at 21:00 UTC (-3 hours) to 29 January at 03:00 UTC (+3 hours). As far as spatial interpolation is concerned, each Argo temperature is directly integrated in the closest RTG grid point employing the nearest-neighbour interpolation scheme (Accadia *et al.*, 2003). Different methods for ingesting Argo temperatures onto gridded RTG have also been tested (e.g. inverse distance weight-IDW) but they provided almost identical to the nearest-neighbour interpolation scheme SST fields. No smoothing or any other filter is integrated in the final RTG-ARGO SST field in order to assess directly the impact of Argo temperatures on numerical weather prediction. Argo temperatures measured in the 0-6 hPa pressure layer (up to ~6 m depth) are considered to be closest to the sea surface and are incorporated in the RTG analyses. The majority (~60%) of the incorporated Argo temperatures measured in the 0-4 hPa pressure layer (up to ~4 m depth) and about 20% measured very close to the sea surface (~0 hPa). Argo temperatures characterized by a low-quality index are excluded from the final dataset.

During the simulation period, 69 near-surface Argo temperature measurements were used by the modelling system with the majority of them being used during the initialization stage on 29 January at 00:00 UTC (7 measurements), on 31 January at 12:00 UTC (8 measurements) and on 1 February at 06:00 UTC (9 measurements). The small ratio (~10^{-3}) of the integrated Argo measurements in the sea grid points of the domain is an indication of the weak spatial impact that Argo temperatures might have on the SST analyses.
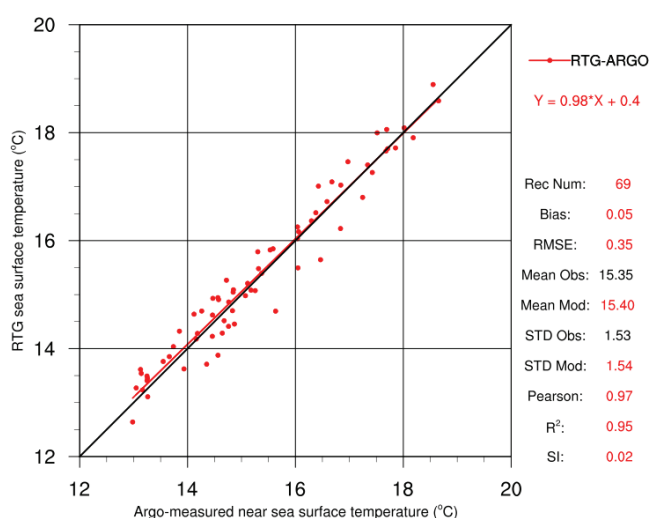
Comparison between the RTG SST analyses and the Argo temperature measurements

The RTG SST gridded analyses are compared with the incorporated Argo temperatures in order to assess their intrinsic biases at the locations of the measurements. In this comparison, the Argo temperatures are considered as reference values because they are in-situ measurements and it is assumed that they are more accurate than the RTG gridded data at the measurement locations. The evaluation methodology is based on a point-to-point hourly comparison between the RTG and the Argo temperatures using the nearest-neighbour interpolation scheme (Accadia *et al.*, 2003; Papadopoulos & Katsafados, 2009). To this end, traditional objective verification scores such as the standard mean error (Bias) and the root mean square error (RMSE) are calculated (Wilks, 1995; Papadopoulos & Katsafados, 2009; Katsafados *et al.*, 2016; Varlas *et al.*, 2018b). The mean value (Mean) and standard deviation (STD) are also calculated for both gridded (depicted as Mean Mod and STD Mod) and measured (depicted as Mean Obs and STD Obs) values. Supplementary scores include the Scatter Index (SI), Pearson's correlation coefficient and the coefficient of determination (R^2).

The differences between RTG and Argo temperatures are in the range of -0.5 to +0.5°C. As shown in Figure 5, RTG slightly overestimates temperature, mainly for temperatures up to 15°C with an overall Bias of 0.05 and RMSE of about 0.35°C. However, RTG and Argo temperatures approach the best fit correlation, with Pearson's coefficient being equal to 0.97. Moreover, the mean values, STD, RMSE, coefficient R^2 and SI indicate good agreement of the two samples. Similar conclusions about the correlation of Argo measurements with SEVIRI retrievals have been drawn by Castro *et al.* (2014).

In order to assess the spatial distribution of Bias and RMSE, the data is analyzed on a grid in horizontal resolution of 2° × 2° (Fig. 6). The temporary positions of Argo floats are superimposed to the error maps and are denoted with black dots. Thus, the errors in each grid cell are extracted from the relevant position of the floats to the grid cell. The pairs of RTG and Argo temperature differences are aggregated in each grid cell of 2° × 2° with the statistical scores colour-shaded over each grid area.

The spatial distribution of Bias indicates RTG overestimation of up to 0.6°C for almost the entire Mediterranean Sea (Balearic Islands, Ionian Sea and south Aegean Sea). A cold Bias in the range of 0.4-0.8°C is evidenced over specific areas in the central Mediterranean such as the Adriatic Sea and the Gulf of Sirte (Fig. 6a). Local RMSE maxima of up to 0.8°C are also evidenced over these areas (Fig. 6b). The overall spatial distribution of RTG Bias does not reveal any distinct geographical pattern or any systematic trend. In the following sections, the impact of those SST differences on the atmospheric conditions between ARGO and CTRL simulations are investigated.
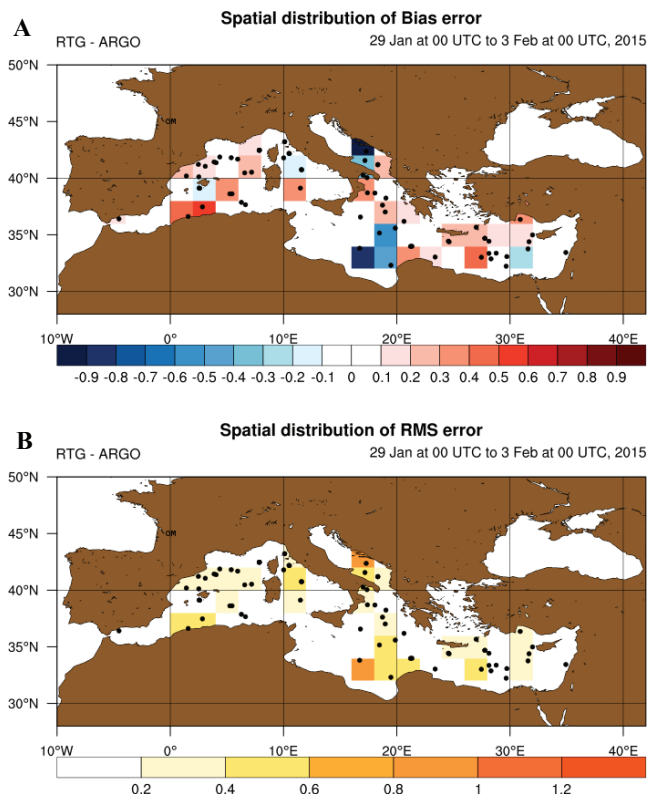

Fig. 5: Scatter plots of sea surface temperature derived from RTG data (y-axis) and near sea surface temperature (°C) measured by Argo floats (x-axis) from 29 January at 00:00 UTC to 3 February at 00:00 UTC, 2015. The pressure layer that was considered for Argo temperature measurements is P = 0-6 mb.

Medit. Mar. Sci., 20/2, 2019, 331-341

335

Fig. 6: Spatial distribution of (a) Bias and (b) RMSE for the period 29 January at 00:00 UTC to 3 February at 00:00 UTC, 2015.

Assessing the response of the atmosphere

The atmospheric response resulting from incorporation of the Argo temperatures is almost negligible, as expected. This is mainly attributed to the small ratio of the integrated values to the sea grid points of the simulation domain. It is already known that surface heat fluxes are intensified over regions with strong SST-air temperature gradients (Fairall *et al.*, 1996, 2003; Iwasaki *et al.*, 2008). Consequently, atmospheric parameters such as MSLP and precipitation may be affected by the modified heat integration mostly over such areas. Nevertheless, even local changes of the SST may affect the air-sea heat transfer and modify the energy budget in a wide area of the marine atmospheric boundary layer (MABL). The generated perturbations of the sea surface heat fluxes propagate according to the synoptic atmospheric conditions and they usually expand their spatial amplitude from local to regional scale (Katsafados *et al.*, 2011). Such a scale transformation alters the spatiotemporal distribution of surface heat fluxes in a non-linear way and finally modifies the MABL thermodynamic structure.

Indeed, Figure 7 (a-c) presents MSLP and precipitation differences between the ARGO and CTRL simulations on 31 January at 00:00 UTC, during the passage of the cyclone over western Greece. Local changes in SST modulate the spatiotemporal distribution of the latent heat flux, which finally modifies the MSLP and precipitation patterns. Three hours earlier, on 30 January at 21:00 UTC, the latent heat flux differences between the ARGO and CTRL simulations approached ±80 W m^{-2} over the Northern Ionian Sea (Fig. 7d). At the same time, the surface sensible heat flux response was much lower. The higher response of the latent heat flux to the incorporation of Argo temperatures is attributed not only to the direct changes in the SST-air temperature gradients but also to the indirect modification of evaporation, which is affected by SST-air temperature gradients. In any case, it is well-known that the heat budget of water vapour determines the latent heat flux (Fairall *et al.*, 1996, 2003;
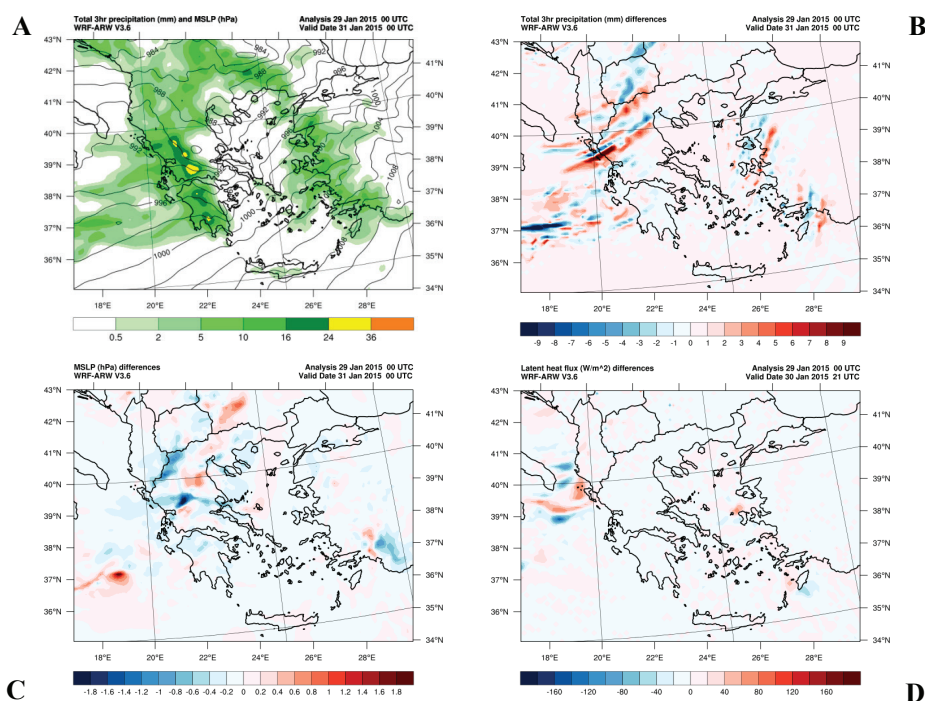

Fig. 7: Spatial distribution of (a) CTRL 3-hourly accumulated precipitation (mm), (b) 3-hourly accumulated precipitation (mm) differences and (c) MSLP (hPa) differences between ARGO and CTRL simulations on 31 January at 00:00 UTC, 2015. (d) Surface latent heat flux (W m^{-2}) differences between ARGO and CTRL simulations on 30 January at 21:00 UTC, 2015.

336

Medit. Mar. Sci., 20/2, 2019, 331-341

Table 2. CTRL and ARGO MSLP (hPa) minima as well as their differences every 12 hours from initialization.

Hours from Initialization (UTC)	CTRL MSLP Minima (hPa)	ARGO MSLP Minima (hPa)	ARGO-CTRL Differences (hPa)
12	987.42	987.32	-0.1
24	974.92	974.87	-0.05
36	966.52	966.61	0.09
48	971.72	971.88	0.04
60	981.51	981.51	0
72	981.2	981.1	-0.1
84	982.28	981.7	-0.58
96	990.11	990.14	0.03
108	993.17	993.27	0.1
120	993.66	994.27	0.61

Zhang *et al*., 2008). The perturbations in the latent heat flux unveil an additional impact of the incorporation of Argo temperatures on the water vapour content of the cyclone. Hence, the SST-air temperature differences and the evaporation yielded by the ARGO simulation have a synergistic effect, which may modify the dynamic and thermodynamic characteristics of the cyclone.

As far as precipitation is concerned, the differences are mainly located over the areas with rain maxima, forming positive and negative bands (Fig. 7b). This is partially attributed to the direct impact of surface heat fluxes on the cyclonic characteristics over the Ionian Sea. Furthermore, the sequence of positive and negative differences is an indication of cyclone track change, represented by the location of MSLP minima (Miglietta *et al*., 2015; Varlas *et al*., 2018a; Katsafados *et al*., 2018). The issue that arises at this point is to investigate whether Argo temperatures can modify the intensity and the track of a cyclone.

Direct ingestion of Argo temperatures in the gridded SST fields modifies the surface heat fluxes and affects the spatiotemporal distribution of the MSLP, as depicted in Figure 7c. In this respect, ARGO temperatures indirectly impact the MSLP minima and even the phase speed of cyclone propagation over the Balkan Peninsula. Indeed, the ARGO simulation presents a faster easterly propagation of the minimum MSLP core and, subsequently, of the cyclonic system from 30 January at 12:00 UTC to 3 February at 00:00 UTC (Fig. 8). In Figure 8, the four-digit numbers include time information. The first two digits represent the day of the month and the other two numbers symbolize the time in UTC. During the previous 36 simulation hours, the MSLP minima locations remained almost identical. Nevertheless, track modification is dependent on the evolution phase of the system and such mechanisms are characterized by increased uncertainty as they are mainly modulated by complex and non-linear processes. It is, thus, difficult to draw conclusions regarding any systematic effect of Argo temperature integration on cyclonic characteristics.

Table 2 presents the CTRL and ARGO MSLP minima as well as their differences every 12 hours from 29 January at 00:00 UTC to 3 February, 00:00 UTC (120 hours in total). Both simulations estimate a MSLP minimum approximately 966.5 hPa on 30 January at 12:00 UTC over
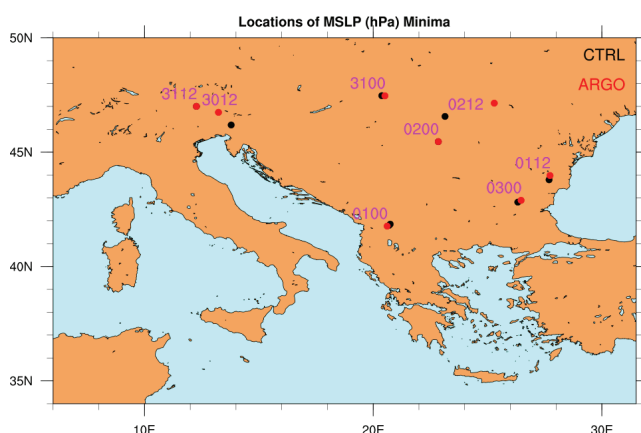

Fig. 8: MSLP (hPa) minima locations, from 30 January at 12:00 UTC to 3 February at 00:00 UTC, 2015. CTRL, and ARGO results are shown in black and red colour, respectively. The four-digit numbers include time information. The first two digits represent the day of the month and the other two symbolize the time in UTC.
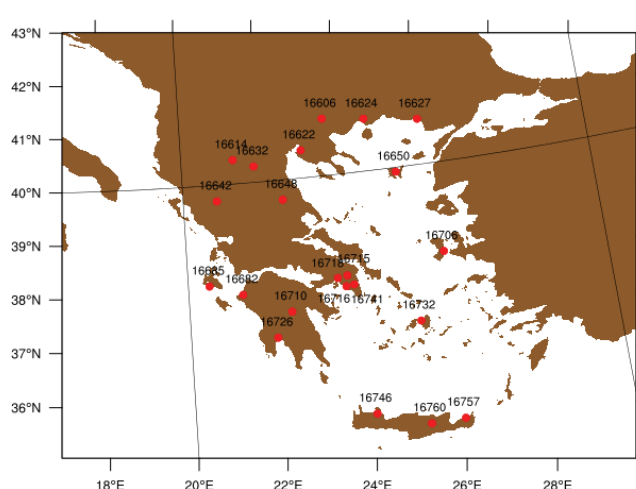

Fig. 9: Locations of the 22 Greek land surface stations of the World Meteorological Organization network considered in the evaluation.

Medit. Mar. Sci., 20/2, 2019, 331-341

337

Table 3. Overall Bias and RMSE at the locations of the surface meteorological stations for near surface wind speed (m s⁻¹), near surface temperature (°C) and MSLP (hPa).

Simulation Mode	Wind speed (m s⁻¹)		Air temperature (°C)		MSLP (hPa)	
	Bias	RMSE	Bias	RMSE	Bias	RMSE
CTRL	0.59	1.83	-1.11	1.96	-0.52	1.39
ARGO	0.60	1.83	-1.10	1.95	-0.51	1.39

north-eastern Italy (Table 2, Fig. 8). While the location of the MSLP minimum is in good agreement with the location yielded by the UK surface analysis (Fig. 2b), both simulations estimate an ~8 hPa deeper cyclone at this time. In general, no systematic effect on the MSLP minima of the cyclone has been evidenced. The differences (ARGO-CTRL) in MSLP minima are below ±1 hPa and range from -0.58 to +0.61 hPa.

Statistical evaluation

Both simulations have been evaluated over land against records from the network of the Hellenic surface stations provided by the World Meteorological Organization. The location of the 22 stations included in the evaluation and their spatial distribution are illustrated in Figure 9. The meteorological variables considered in the evaluation are: near surface wind speed, the near surface temperature, MSLP and accumulated precipitation.

The evaluation methodology is based on point-to-point hourly comparison between model-generated variables and the observations (Wilks, 1995). The gridded outputs are interpolated to each location using the nearest-neighbour interpolation scheme. Consequently, many pairs of model outputs and observations are produced for both the CTRL and ARGO runs. Advanced quality control has also been applied in order to remove the erroneous observations, based on checking the physical range of each parameter being verified, the allowable rate of change in time and stationarity. The abovementioned verification scores (Bias, RMSE, Mean, STD, SI, Pearson and R^2) are calculated for the main continuous parameters (wind speed, temperature and MSLP). The verification scores used for the discrete variable (precipitation) are based on the contingency table approach (Wilks, 1995). This is a two-dimensional matrix where each element counts the number of occurrences in which the observations and the model forecasts exceeded or failed to reach a certain threshold for a given forecast period (Papadopoulos & Katsafados, 2009). The forecast skill can be estimated using the contingency table in order to calculate the bias score (BIAS), the equitable threat score (ETS), the RMSE and the Heidke skill score (HSS). More details about these statistical scores are available in Papadopoulos *et al.* (2005) and Papadopoulos & Katsafados (2009).

The scatter plots and the statistical scores also confirm the negligible impact of Argo temperature integration on the forecast skill over land (Table 3, Fig. 10). In more details, near surface wind speed over 12 m s⁻¹ is overestimated with bias scores of 0.59 m s⁻¹ and 0.60 m s⁻¹ for the

CTRL and ARGO simulation, respectively. Near surface temperature above 5°C is mainly underestimated with bias scores of -1.11°C and -1.10°C, respectively. MSLP above 995 hPa is slightly overestimated with an identical RMSE of 1.39 hPa for both simulations. Mean value, STD, Pearson, R^2 and SI present similar performance for ARGO and CTRL simulations (Fig. 10). Temperature and MSLP underestimation as well as wind speed overestimation are also in agreement with previous studies investigating the WRF model performance (*e.g.* Katsafados *et al.*, 2011). The abovementioned latent heat flux differences, which are shown in Figure 7, are not propagated over remote land areas and therefore do not primarily affect the forecast skill of MSLP, near surface temperature and wind speed.

The evaluation of the 6-hour accumulated precipitation is performed for 6 predefined precipitation thresholds (0.5, 1, 2, 4, 6 and 8 mm). In general, both simulations overestimate precipitation (Fig. 11a) while the impact of local SST changes on the precipitation forecast skill is not considered significant (Fig. 11a-d). Nevertheless, the ARGO simulation slightly reduces the Bias of the medium and higher thresholds (Fig. 11a). ETS and HSS reduce with the increase of thresholds presenting a slight improvement for the ARGO run (Figs. 11b, c). The ARGO simulation presents a slightly better performance in RMSE, offering a decrease of up to 3% in medium and high thresholds despite the fact that RMSE increases with the amount of precipitation in both simulations (Fig. 11d).

Conclusions

In this study, the impact of the sea surface temperatures measured by the Argo floats on the NWP forecast skill is primarily assessed through a simulation of an extreme weather event over the Eastern Mediterranean Sea. A case study of a high-impact weather event in the period from 29 January to 3 February 2015 was selected due to the severity of the atmospheric conditions that prevailed mainly over Greece. Two sensitivity simulations were conducted; the first one (CTRL) employing RTG gridded SST analyses and the second one (ARGO) additionally incorporating Argo temperature measurements in the RTG SST analyses for the generation of initial and lower boundary conditions. With the Argo measurements as a reference, the RTG gridded analyses slightly overestimate SST temperatures covering almost the entire Mediterranean Sea (Balearic Islands, Ionian Sea and south Aegean Sea). A few cold bias spots are also evidenced over specific areas in the central Mediterranean such as
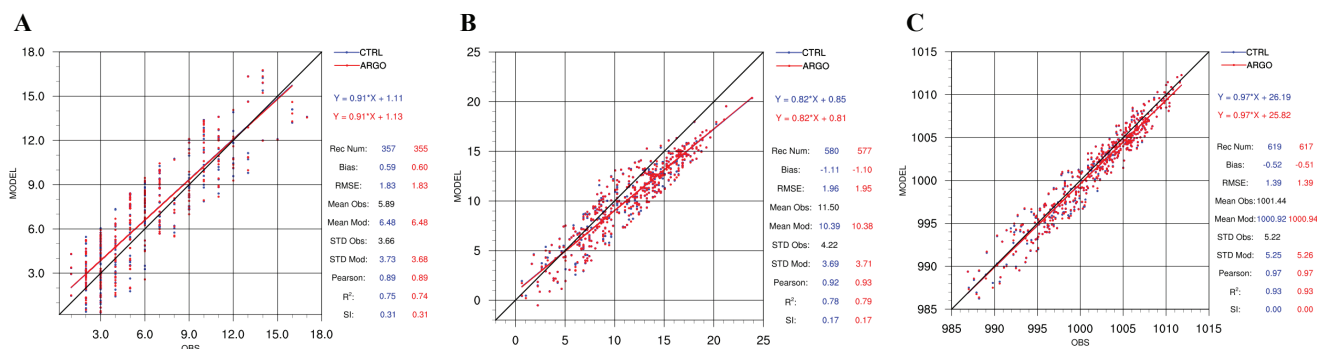
338

Medit. Mar. Sci., 20/2, 2019, 331-341

Fig. 10: Scatter plots for the CTRL and ARGO experiments for (a) near surface wind speed (m s^{-1}), (b) near surface temperature (°C) and (c) MSLP (hPa). The Y-axis represents the model-estimated values and the X-axis the surface observations. CTRL and ARGO evaluation results are shown in blue and red colour, respectively.

the Adriatic Sea and the Gulf of Sirte.

Both simulations produced almost identical results due to the limited number of Argo temperature measurements incorporated in the ARGO simulation. An additional explanation for these results between the two simulations is that the RTG data realistically represent the SST fields thus minimizing the differences with in-situ data such as Argo temperatures. Therefore, wind speed and temperature seem to be negligibly affected by the integration of Argo temperatures. However, the spatial and temporal distributions of surface heat fluxes, MSLP and precipitation are slightly perturbed by Argo temperature integration. Local changes in SST affected the spatiotemporal distribution of the latent heat flux, which finally modified the MSLP and precipitation patterns. The latent heat flux differences are in the range of ±80 W m^{-2} and their maxima are also linked with the precipitation maxima. Additionally, the modification of surface heat fluxes modulated the track of the cyclone. Thus, ARGO simulation is mainly characterized by the faster easterly propagation of the cyclonic system, which is more prominent after 36 simulation hours. However, such outcomes are characterized by increased uncertainty because the key mechanisms are mainly determined by complex and nonlinear processes. It is, thus, difficult to draw conclusions regarding any systematic influence of Argo temperature integration on the cyclonic thermodynamic structure.

The forecast skill of the two simulations is statistically evaluated against land surface observations over Greece using the point-to-point hourly comparison methodology. The ARGO simulation offered an up to 3% improvement in the precipitation scores, more prominent in the range from medium to high precipitation thresholds. However, the basic scores of the other continuous variables remain almost identical. Although these preliminary results are promising, the authors' future plans are aimed at incorporating a larger sample of ARGO measurements in additional simulations as well as including advanced assimilation methods in more case studies under diverse atmospheric synoptic conditions.
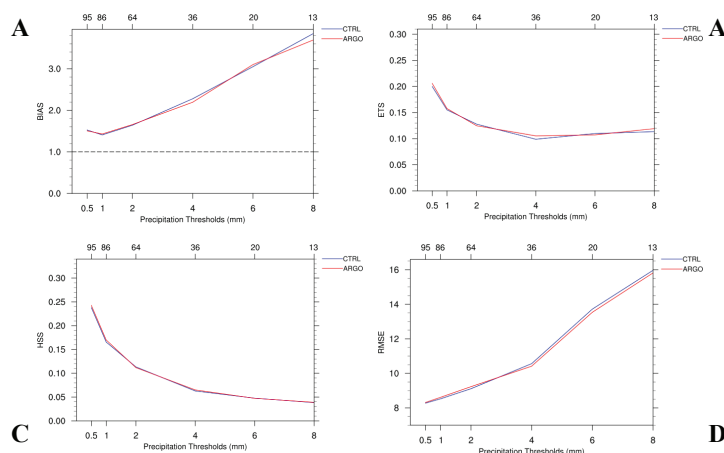
Fig. 11: (a) Bias, (b) ETS, (c) HSS and (d) RMSE scores for the CTRL (blue line) and the ARGO (red line) simulations for specific precipitation thresholds. The numbers above tick marks denote the sample for each corresponding threshold value.

Medit. Mar. Sci., 20/2, 2019, 331-341

339

gratefully acknowledged for the provision of operational analyses. Finally, the Argo data were collected and made freely available by the International Argo Program and the national programs that contribute to the Program (http://www.argo.ucsd.edu, http://argo.jcommops.org). The Argo Program is part of the Global Ocean Observing System.

References

Accadia, C., Mariani, S., Casaioli, M., Lavagnini, A., Speranza, A., 2003. Sensitivity of precipitation forecast skill scores to bilinear interpolation and a simple nearest-neighbor average method on high-resolution verification grids. *Weather and Forecasting*, 18 (5), 918-932.

Argo, 2000. Argo float data and metadata from Global Data Assembly Centre (Argo GDAC). SEANOE.

Balmaseda, M., Anderson, D., 2009. Impact of initialization strategies and observations on seasonal forecast skill. *Geophysical Research Letters*, 36 (1).

Balmaseda, M., Anderson, D., Vidard, A., 2007. Impact of Argo on analyses of the global ocean. *Geophysical Research Letters*, 34 (16).

Castro, S.L., Wick, G.A., Buck, J.J., 2014. Comparison of diurnal warming estimates from unpumped ARGO data and SEVIRI satellite observations. *Remote Sensing of Environment*, 140, 789-799.

Christakos, K., Cheliotis, I., Varlas, G., Steeneveld, G.J., 2016. Offshore wind energy analysis of cyclone Xaver over North Europe. *Energy Procedia*, 94, 37-44.

Christakos, K., Varlas, G., Reuder, J., Katsafados, P., Papadopoulos, A., 2014. Analysis of a low-level coastal jet off the western coast of Norway. *Energy Procedia*, 53, 162-172.

Fairall, C.W., Bradley, E.F., Hare, J.E., Grachev, A.A., Edson, J.B., 2003. Bulk parameterization of air–sea fluxes: Updates and verification for the COARE algorithm. *Journal of Climate*, 16 (4), 571-591.

Fairall, C.W., Bradley, E.F., Rogers, D.P., Edson, J.B., Young, G.S., 1996. Bulk parameterization of air-sea fluxes for tropical ocean-global atmosphere coupled-ocean atmosphere response experiment. *Journal of Geophysical Research: Oceans*, 101 (C2), 3747-3764.

Gemmill, W., Katz, B., Li, X., 2007. Daily Real-Time Global Sea Surface Temperature - High Resolution Analysis at NOAA/NCEP. *NOAA / NWS / NCEP / MMAB Office Note Nr*, 260, 39.

Gopalakrishnan, S.G., Goldenberg, S., Quirino, T., Zhang, X., Marks Jr, F. *et al.,* 2012. Toward improving high-resolution numerical hurricane forecasting: Influence of model horizontal grid resolution, initialization, and physics. *Weather and Forecasting*, 27 (3), 647-666.

Hong, S.-Y., Dudhia, J., Chen, S.-H., 2004. A revised approach to ice microphysical processes for the bulk parameterization of clouds and precipitation. *Monthly Weather Review*, 132, 103-120.

Hong, S.-Y., Noh, Y., Dudhia, J., 2006. A new vertical diffusion package with an explicit treatment of entrainment processes. *Monthly Weather Review*, 134, 2318-2341.

Iwasaki, S., Kubota, M., Tomita, H., 2008. Inter-comparison and evaluation of global sea surface temperature products. *International Journal of Remote Sensing*, 29 (21), 6263-6280.

Jiménez, P.A., Dudhia, J., González-Rouco, J.F., Navarro, J., Montávez, J.P. *et al.,* 2012. A revised scheme for the WRF surface layer formulation. *Monthly Weather Review*, 140 (3), 898-918.

Kara, A.B., Barron, C.N., 2007. Fine-resolution satellite-based daily sea surface temperatures over the global ocean. *Journal of Geophysical Res*earch, 112, C05041.

Kassis, D., Korres, G., Konstantinidou, A., Perivoliotis, L., 2017. Comparison of high resolution hydrodynamic model outputs with in-situ Argo profiles in the Ionian Sea. *Mediterranean Marine Science*, 18 (1), 22-37.

Kassis, D., Korres, G., Petihakis, G., Perivoliotis, L., 2015. Hydrodynamic variability of the Cretan Sea derived from Argo float profiles and multi-parametric buoy measurements during 2010-2012. *Ocean Dynamics*, 65(12), 1585-1601.

Kassis, D., Krasakopoulou, E., Korres, G., Petihakis, G., Triantafyllou, G.S., 2016. Hydrodynamic features of the South Aegean Sea as derived from Argo T/S and dissolved oxygen profiles in the area. *Ocean Dynamics*, 66 (11), 1449-1466.

Kassis, D., Perivoliotis, L., Korres, G., 2014. Greek Argo: Towards monitoring the Eastern Mediterranean-First deployments preliminary results and future planning. 7th Euro-GOOS Conference, Lisbon 28-30 October 2014.

Katsafados, P., Mavromatidis, E., Papadopoulos, A., Pytharoulis, I., 2011. Numerical simulation of a deep Mediterranean storm and its sensitivity on sea surface temperature. *Natural Hazards and Earth System Sciences,* 11 (5), 1233-1246.

Katsafados, P., Papadopoulos, A., Kallos, G., 2005. Regional atmospheric response to tropical Pacific SST perturbations. *Geophysical Research Letters*, 32, L04806.

Katsafados, P., Varlas, G., Papadopoulos, A., Spyrou, C., Korres, G., 2018. Assessing the implicit rain impact on sea state during hurricane Sandy (2012). *Geophysical Research Letters*, 45 (21), 12015-12022.

Korres, G., Kassis, D., 2012. National report: "Greek ARGO programme, present status and future plans".

Korres, G., Nittis, K., Hoteit, I., Triantafyllou, G., 2009. A high resolution data assimilation system for the Aegean Sea hydrodynamics. *Journal of Marine Systems*, 77, 325-340.

Korres, G., Nittis, K., Perivoliotis, L., Tsiaras, K., Papadopoulos, A., Hoteit, I., Triantafyllou, G., 2010. Forecasting the Aegean Sea hydrodynamics within the POSEIDON-II operational system. *Journal of Operational Oceanography*, 3 (1), 37-49.

Korres, G., Ntoumas, M., Potiris, M., Petihakis, G., 2014. Assimilating Ferry Box data into the Aegean Sea model. *Journal of Marine Systems*, 140, 59-72.

Krokos, G., Velaoras, D., Korres, G., Perivoliotis, L., Theocharis, A., 2014. On the continuous functioning of an internal mechanism that drives the Eastern Mediterranean thermohaline circulation: The recent activation of the Aegean Sea as a dense water source area. *Journal of Marine Systems*, 129, 484-489.

Le Traon, P.Y., 2013. From satellite altimetry to Argo and operational oceanography: three revolutions in oceanography. *Ocean Science*, 9 (5), 901-915.

Miglietta, M.M., Mastrangelo, D., Conte, D., 2015. Influence

340

Medit. Mar. Sci., 20/2, 2019, 331-341

of physics parameterization schemes on the simulation of a tropical-like cyclone in the Mediterranean Sea. *Atmospheric Research*, 153, 360-375.

Mignac, D., Tanajura, C.A.S., Santana, A.N., Lima, L.N., Xie, J., 2015. Argo data assimilation into HYCOM with an EnOI method in the Atlantic Ocean. *Ocean Science*, 11 (1), 195-213.

Mohanty, U.C., Osuri, K.K., Routray, A., Mohapatra, M., Pattanayak, S., 2010. Simulation of Bay of Bengal tropical cyclones with WRF model: Impact of initial and boundary conditions. *Marine Geodesy*, 33 (4), 294-314.

Nilsson, J.A., Dobricic, S., Pinardi, N., Taillandier, V., Poulain, P.M., 2011. On the assessment of Argo float trajectory assimilation in the Mediterranean Forecasting System. *Ocean Dynamics*, 61 (10), 1475-1490.

Papadopoulos, A., Chronis, T.G., Anagnostou, E.N., 2005. Improving convective precipitation forecasting through assimilation of regional lightning measurements in a mesoscale model. *Monthly Weather Review*, 133 (7), 1961-1977.

Papadopoulos, A., Katsafados, P., 2009. Verification of operational weather forecasts from the POSEIDON system across Eastern Mediterranean. *Natural Hazards and Earth System Sciences,* 9 (4), 1299-1306.

Pielke Sr, R.A., 2013. Mesoscale meteorological modeling (Vol. 98). *Academic press*.

Reynolds, R.W., Rayner, N.A., Smith, T.M., Stokes, D.C., Wang, W., 2002. An improved in situ and satellite SST analysis for climate. *Journal of Climate*, 15 (13), 1609-1625.

Roemmich, D., Gilson, J., 2009. The 2004-2008 mean and annual cycle of temperature, salinity, and steric height in the global ocean from the Argo Program. *Progress in Oceanography*, 82 (2), 81-100.

Skamarock, W.C., Klemp, J.B., Dudhia, J., Gill, D.O., Barker, D. *et al.,* 2008. A Description of the Advanced Research WRF Version 3, *NCAR Technical Note*, TN-468+STR, 113 pp.

Tewari, M., Chen, F., Wang, W., Dudhia, J., LeMone, M.A. *et al.,* 2004. Implementation and verification of the unified NOAH land surface model in the WRF model. Proc. of 20th Conf. on Weather Anal. and Forecast./16th Conf. on Numer. Weather Predict. 12-16 January 2004, Seattle, USA, pp. 2165-2170.

The Argo Science Team, 1998. On the design and implementation of Argo: an initial plan for a global array of profiling floats. International CLIVAR Project Office Report 21, GODAE Report 5. GODAE International Project Office, Melbourne, Australia, 32 pp.

Thiébaux, J., Rogers, E., Wang, W., Katz, B., 2003. A new high-resolution blended real-time global sea surface temperature analysis. *Bulletin of the American meteorological Society*, 84 (5), 645-656.

Tonani, M., Oddo, P., Korres, G., Clementi, E., Dobricic, S. *et al.,* 2014. The Mediterranean Forecasting System: recent developments. In EGU General Assembly Conference Abstracts. p. 16899.

Varlas, G., Papadopoulos, A., Katsafados, P., 2018a. An analysis of the synoptic and dynamical characteristics of hurricane Sandy (2012), Meteorology and Atmospheric Physics, 1-11.

Varlas, G., Katsafados, P., Papadopoulos, A., Korres, G., 2018b. Implementation of a two-way coupled atmosphere-ocean wave modeling system for assessing air-sea interaction over the Mediterranean Sea. *Atmospheric Research*, 208, 201-217.

Varlas, G., Papadopoulos, A., Nomikou V.M., Karymbalis, E., Anagnostou, M. *et al.,* 2018c. Assessing the interaction between the atmospheric and hydrological environments in the drainage basin of Spercheios River, 14th International Conference on Meteorology, Climatology and Atmospheric Physics (COMECAP), October 15-17, 2018, Alexandroupolis, Greece.

Velaoras, D., Krokos, G., Nittis, K., Theocharis, A., 2014. Dense intermediate water outflow from the Cretan Sea: A salinity driven, recurrent phenomenon, connected to thermohaline circulation changes. *Journal of Geophysical Research: Oceans*, 119 (8), 4797-4820.

Wilks, S., 1995. Statistical Methods in the Atmospheric Sciences, *Academic Press*, 233-242.

Xie, J., Zhu, J., 2010. Ensemble optimal interpolation schemes for assimilating Argo profiles into a hybrid coordinate ocean model. *Ocean Modelling*, 33 (3), 283-298.

Zhang, J.A., Black, P.G., French, J.R., Drennan, W. M., 2008. First direct measurements of enthalpy flux in the hurricane boundary layer: The CBLAST results. *Geophysical Research Letters*, 35 (14).

Medit. Mar. Sci., 20/2, 2019, 331-341

341